

Fine-resolution wavelet analysis of exoplanetary distributions: hints of an overshooting iceline accumulation

Roman V. Baluev^{1,2*} and Vakhit Sh. Shaidulin²

¹Central Astronomical Observatory at Pulkovo of Russian Academy of Sciences, Pulkovskoje shosse 65/1, St Petersburg 196140, Russia

²Saint Petersburg State University, Universitetskij prospekt 28, Petrodvorets, St Petersburg 198504, Russia

in original form 2017 December 15

ABSTRACT

We investigate 1D exoplanetary distributions using a novel analysis algorithm based on the continuous wavelet transform. The analysis pipeline includes an estimation of the wavelet transform of the probability density function (p.d.f.) without pre-binning, use of optimized wavelets, a rigorous significance testing of the patterns revealed in the p.d.f., and an optimized minimum-noise reconstruction of the p.d.f. via matching pursuit iterations.

In the distribution of orbital periods, P , our analysis revealed a narrow subfamily of exoplanets within the broad family of “warm jupiters”, or massive giants with $P \gtrsim 300$ d, which are often deemed to be related with the iceline accumulation in a protoplanetary disk. We detected a p.d.f. pattern that represents an upturn followed by an overshooting peak spanning $P \sim 300 - 600$ d, right beyond the “period valley”. It is separated from the other planets by p.d.f. concavities from both sides. It has at least two-sigma significance.

In the distribution of planet radii, R , and using the California Kepler Survey sample properly cleaned, we confirm the hints of a bimodality with two peaks about $R = 1.3R_{\oplus}$ and $R = 2.4R_{\oplus}$, and the “evaporation valley” between them. However, we obtain just a modest significance for this pattern, two-sigma only at the best. Besides, our follow-up application of the Hartigan & Hartigan dip test for unimodality returns 3 per cent false alarm probability (merely 2.2-sigma significance), contrary to 0.14 per cent (or 3.2-sigma), as claimed by [Fulton et al. \(2017\)](#).

Key words: methods: data analysis - methods: statistical - astronomical data bases: miscellaneous - planetary systems - stars: statistics

1 INTRODUCTION

A great diversity of extrasolar planets was discovered over the last two decades. After the detection of the first “hot jupiter” orbiting 51 Pegasi ([Mayor & Queloz 1995](#)), the number of known exoplanets grew with an increasing rate, and presently, according to *The Extrasolar Planets Encyclopaedia* ([Roques & Schneider 1995](#)), it reached the milestone of 3000.

Such a number of objects represents a huge interest from the statistical point of view. The exoplanetary statistics is capable to provide a lot of invaluable information, in particular with a concern to planet formation and evolution theories ([Cumming 2010](#)).

There are several recognized statistical features in exoplanetary distributions that were known long ago. For example, in the orbital periods distribution the following large-

scale patterns appear: (i) the subfamily of “hot jupiters” (HJ hereafter) at the short-period edge of the distribution, (ii) the “period valley” (PV) that represents a wide depression in the period range $P \sim 10 - 300$ d, (iii) the dominant maximum of “warm jupiters” (WJ) with $P \gtrsim 300$ d. The latter one also incorporate more “cold” long-period objects like Jupiter in the Solar System. These statistical patterns were more or less successfully reproduced in planet formation and migration models ([Ida & Lin 2004, 2008](#)).

In particular, the WJ family is usually treated as an evidence in favour of the effect of the iceline barrier that stimulates the planet formation near the frost edge, where the water starts to condensate in ice in a protoplanetary disk. In the Solar protoplanetary disk, the ice line was situated about ~ 2.7 AU from the Sun ([Hayashi 1981](#)), and this would correspond to the Keplerian orbital period of $P \sim 1600$ d. This appears much larger than the value of $P \sim 300$ d mentioned above, but giant planets, which are predominant in that statistics, additionally undergo the type-II migration

* E-mail: r.baluev@spbu.ru

that brings their final position inward relatively to the actual iceline (Ida & Lin 2008; Schlaufman et al. 2009).

In multiple works many other apparent statistical features in the exoplanetary ensemble are noticed sometimes. However, they often lack a good justification in terms of the statistical significance. Indeed, it is not easy to supply a formal statistical support (like e.g. a p-value) in favour of a hypothesis that there is a subfamily of objects with given characteristics. This would require sophisticated mathematics, something like cluster analysis with a rich statistical content. Due to this difficulty, mostly the large-scale structures remain undoubtful in the exoplanetary statistics, like those described above in the orbital periods distribution.

In this work we set a goal to perform a *fine-resolution* analysis of exoplanetary distributions. That is, we seek to detect small-scale features in their statistics. For this, we apply our newly-developed wavelet analysis algorithm (Baluev 2017). It was designed to detect patterns belonging to the following basic classes: quick density gradients, convexities and concavities of the probability density function (p.d.f.). In a less formal wording, the method would be helpful in revealing transitions between statistical families, these families themselves, and separations between.

Basically, this paper also represents the first effort to perform a field-test of that analysis algorithm. Our goal is to perform a systematic investigation of different exoplanetary distributions and to decide in a uniform way, what p.d.f. details are significant there and which are not.

The structure of the paper is as follows. In Sect. 2 we discuss some important issues that often render statistical analysis unreliable and untrustable, and how to fight them. In Sect. 3 we provide a brief description and justification of the algorithm. In Sect. 4 we described how we constructed exoplanetary samples to be analysed. Finally, Sect. 5 presents results of the analysis for different exoplanetary characteristics.

2 AVOID DATA-DRIVEN ANALYSIS, BEWARE OF MULTIPLE TESTS, AVOID P-HACKING!

Mathematical statistics provides us with great tools that finally make scientific results more trustable. This is achieved by filtering out insignificant conclusions likely inspired by noise. However, in practice statistical methods are frequently used formally or wrongly, violating their necessary prerequisite conditions of applicability. Such a violation is often hidden implicitly and is not obvious to a researcher. But regardless of that, the results of the analysis become statistically invalid, though still pretty convincing for a quick external view. Often, this hidden poison of false reliability reveals itself only when new data are acquired. Previous interpretations, even those that deemed significant, are often disavowed or transformed drastically on the basis of new data. As a result, the trust to justifications based on statistical inference become diluted.

This phenomenon of the “untrusted significance” poisons all science branches that deal with noisy or random data, in particular astronomy and astrophysics.

A good example demonstrating quick change in the interpretation regardless of its previous significance, is pro-

vided by an exoplanetary system GJ 581. A few years ago, it was a matter of intensive disputes, when different teams and individual authors reported distinct sets of up to six planets. Combining different radial velocity data, they derived different interpretations that could not be all consistent with each other (Vogt et al. 2010; Gregory 2011; Forveille et al. 2011; Tadeu dos Santos et al. 2012; Vogt et al. 2012). Definitely, these authors were not ignorant of the significance and provided apparently convincing statistical treatment. But these “iterations” nevertheless did not converge to a definite and convincing solution. The situation was somewhat clarified with the work (Baluev 2013a), where it was shown that most of the problems come from the correlated noise polluting Doppler data. Taking the red noise into account, only three candidate planets *b*, *c*, and *e*, demonstrated undoubtful detection significance, two candidates *f* and *g* were rejected as likely noise artifacts, while the planet *d* remained questioned (two-sigma significance at the best).

Later on, the significance of this planet *d* signal was redetermined to be above three-sigma (Baluev 2015), while the previous too low estimate was attributed to the effect of mathematical singularities in the adopted noise model. But simultaneously, another research group (Robertson et al. 2014, 2015) claimed that the Doppler signal previously attributed to the putative planet *d* is actually a result of stellar activity. In particular, their analysis revealed correlations of this signal with a spectral activity indicator.

However, Anglada-Escudé et al. (2016) showed that the analysis performed by Robertson et al. (2014) appeared deficient and flawed from the statistical point of view. The mistake appeared because the best-fit residuals to a multiparametric model were computed and then used as input data to test for correlation with stellar activity. But the correlation test was not designed for such a usage. It is obvious that best-fit residuals are always systematically biased, because any fitting algorithm seeks to reduce them. Hence, the simplistic correlation test returned a much higher significance than it really was. Correct analysis made by (Anglada-Escudé et al. 2016) did not reveal significant correlation with the activity indicator.

Speaking in a more formal wording, the mistake appeared, because a statistical test designed to test *simple* null hypothesis was misapplied to a hypothesis of *complex* type. This appears to be a rather common type of mistakes in statistical testing. For example, the famous Kolmogorov-Smirnov distribution goodness-of-fit test, regardless of the word “fit” in its title, should never be used to test the goodness of a *fitted* model. The null distribution must be specified completely for this test to be valid. All parameters of the model, if any, must be specified *prior* to the first look at the data. At least, they should not be fitted with *the same* data.

This prerequisite condition is violated frequently, because practical models always have some parameters. Prior to any testing, a researcher often has to estimate them, at least by a visual look at the empiric histogram. But in such a case, the significance levels of the classic K–S test must be recalibrated to take into account these hidden, “subconscious”, degrees of freedom. Otherwise we increase the risk to wrongly conclude that the empiric distribution has a good agreement with the model.

Investigating the problem further, we may realize that

mistakes generally similar to the ones just described are made quite frequently. Gelman & Loken (2014) give a brief but very clear example-based presentation of the issue. In general, mistakes come from hidden degrees of freedom that are processed either subconsciously or in some pre-analysis or pre-selection procedure. Gelman & Loken (2014) call it “data-driven analysis” and “p-hacking”.

Summarizing Gelman & Loken (2014), it is a bad practice to:

(i) Use parametrized model in a test that was designed to handle non-parametric models or models with a smaller number of parameters. As discussed above, this includes cases when additional parameters are estimated “on the fly” or “subconsciously”.

(ii) Formulate comparison hypotheses or models *post-hoc*, i.e. based on the empiric data, and then process these same data with a test that remains “unaware” of such a preanalysis (i.e., was not designed specifically to handle it).

(iii) Perform a large number of similar tests, varying some parameters. In particular, varying them over a grid, since this is an implicit version of point (i).

(iv) Select a very specific test only to verify a specific hypothesis emerged after some pre-analysis or even just the first look on the same data. Such a practice might look quite innocently, but it turns to be a version of point (ii).

(v) Start the analysis without clear understanding of what question we ask to the data and without a clear set of possible hypotheses or models. It is admissible if in the beginning of some new research we want to detect just something interesting, but then this “just something interesting” must be more or less formalized and the set of possible outcomes should be clearly outlined (though it must remain wide). This need to be done in advance of the analysis, or it won’t be trustable due to point (ii).

(vi) Assume that a low false alarm probability guarantees the same low fraction of false alarms in our output results, even if all validity conditions of our test were pedantically satisfied. The problem is that usually only “positive” results (or “alarms”) are published, and all other data, that appeared not so attractive, remain hidden. If $N = 100$ stars were investigated, and $n = 10$ of them were found to have a planet with $FAP = 1$ per cent significance, this means we should expect about $N FAP = 1$ false positives. This would be the whole 10 per cent of the output list of n candidates, and this is much larger than $FAP = 0.01$ originally requested.

Unfortunately, the astronomical literature is not free from hidden mistakes of these types. After the example if GJ 581, let us move closer to the primary topic of the present paper, or the analysis of exoplanetary distributions. Wright et al. (2009) provided a set of distribution comparisons between planets orbiting in multiplanet and single-planet systems. They reported a lot of positive results. Based on the two-sample Kolmogorov-Smirnov test, they claimed statistically significant differences between the single- and multi-planet distributions of semimajor axes, masses, eccentricities.

We did not verify how likely these particular conclusions are in view of the contemporary exoplanets data, but we draw attention to the analysis performed in (Wright et al. 2009), which appears definitely flawed. The method is de-

tailedly described in their paper appendix, and it reveals the following mistakes:

(i) The p-values for the K–S two-sample D -statistic are computed from Monte Carlo simulations rather than by the classic analytic approximation. Perhaps the authors tried to reach more reliability, but this triggered an opposite effect. A hidden flaw was that the p-values were simulated from the *observed*, or *empiric*, sample of single planets. But this implies that their null hypothesis referred to a *discontinuous* cumulative distribution function. And it is well-known that the distribution of the K–S statistic for a discontinuous null hypothesis can be different from the common continuous case. Moreover, this discontinuity appears completely artificial: it is unrelated to any “physical” discontinuity that a given underlying distribution might by any means involve.

(ii) The p-values are computed separately for positive, D^+ , and negative, D^- , outcomes of the K–S D -statistic, based on their corresponding distribution functions. But this is the case of a direct p-hacking and data-driven analysis. Indeed, it was *a priori* unknown, which statistic, D^+ or D^- , would result in a larger value. In actuality, the two-sided test statistic $D = \max(|D^+|, |D^-|)$ was computed rather than either of the single-sided ones. And it was illegal to use single-sided p-values with actually two-sided statistic. This seems to be the most important mistake that roughly halved the estimated value of the FAP, making the results falsely more significant than they really are.

(iii) Apparently, the random nature of the basic sample of single planets (that was used to simulate p-values) was not taken into account at all. The description mentions that the multiplanet distributions were simulated, but not the single-planet ones, which instead served as a fixed null-hypothesis reference. This means that the authors actually applied the usual one-sample K–S test rather than the two-sample one. They just set up the empiric distribution of the single planets as the null hypothesis for the classic K–S test. Such a replacement implies a minor underestimation in the D -statistic threshold levels by the factor of $\sqrt{1 + m/n} \simeq 1.14$, where $m = 67$ and $n = 230$ are the number of planets in the comparison samples from their work.

The best solution in this case would be to just stick with the classic analytic approximation for the two-sample K–S test. The largest value of D^\pm statistic reported by Wright et al. (2009) was $D^+ = 2.06$ (for the eccentricity distribution), and its correct p-value becomes $FAP = 0.04$ per cent, still indicating a convincingly significant discrepancy. But the next large value was $D^+ = 1.36$ (for the mass distribution), resulting in $FAP = 5$ per cent, which is considerably larger than the original simulated estimate of 1.8 per cent.

Yet another work not free from a hidden data-driven analysis was published recently by Fulton et al. (2017). It is discussed below in Sect. 5.2.

We summarize our understanding of how to avoid unreliable statistical results via a citation from (Gelman & Loken 2014): “For a p-value to be interpreted as evidence, it requires a strong claim that the same analysis would have been performed had the data been different.” And what should be treated as a bad practice, is “data-dependent analysis choices that did not appear to

be degrees of freedom because the researchers analyze only one data set at a time.”

We finish this section with a note that although all the above discussion relied on such a purely frequentist notion like p-value, Bayesian methods are equally sensitive to these issues. The main difference between the Bayesian and frequentist methods is in the metric that they utilize to order statistical decisions. But examples above owe to a wrongly formulated statistical model that hiddenly involved more degrees of freedom and more uncertainty than the analysis assumed.

3 DESCRIPTION OF THE ALGORITHM

In (Baluev 2017), a self-consistent pipeline of the statistical wavelet analysis is described. In view of what is said in Sect. 2 concerning the danger of data-driven analysis and hidden degrees of freedom, we need to highlight some advantages of this pipeline.

Just like the most of other well-formulated statistical tools, our method is supposed to be applied *blindly*, i.e. without any preanalysis of the input data. But even if some preanalysis was done, our algorithm scans all possible structures anyway, allowing for a very wide set of their characteristics. In other words, its set of test hypotheses is inherently wide, and relatively little space is left for hidden degrees of freedom. In some sense, wavelets offer one possible formalization of a vague task “to find something interesting” in the distribution, avoiding too narrow specification of this “something interesting”.

The algorithm is aimed to analyse only single-dimensional random samples. The mathematical details are given in (Baluev 2017), and a brief step-by-step explanation of the method follows below.

(i) We use the wavelets called as CBHAT (“cowboy hat”) and WAVE2 that represent optimized modifications of the classic MHAT (“Mexican hat”) and WAVE wavelets. Just like WAVE and MHAT can be obtained by differentiating a Gaussian once or twice, the new optimal wavelets ψ can be produced as derivatives of bell-like generating functions φ :

$$\psi_{\text{WAVE2}}(t) = \varphi'_{\text{WAVE2}}(t), \quad \psi_{\text{CBHAT}}(t) = \varphi''_{\text{CBHAT}}(t). \quad (1)$$

Such wavelet transforms would highlight zones where the first or second derivative of the p.d.f. is large, revealing specific patterns like quick density gradients or p.d.f. convexities and concavities. The latter can be associated with clumps and gaps in the input sample.

(ii) The continuous wavelet transform (CWT) of the p.d.f. $f(x)$ is estimated from the random sample $\{x_i\}_{i=1}^N$:

$$Y(a, b) = \int_{-\infty}^{+\infty} \psi\left(\frac{x-b}{a}\right) f(x) dx$$

estimated by $\tilde{Y}(a, b) = \frac{1}{N} \sum_{i=1}^N \psi\left(\frac{x_i-b}{a}\right).$ (2)

Using similar formulae, the variance of \tilde{Y} is estimated too, in each point (a, b) .

(iii) With \tilde{Y} and its variance estimate, and also based on some comparison model Y_0 (possibly zero on start), a

normalized function $z(a, b)$ is constructed. This z basically represents the Student t -statistic that have approximately constant noise properties over different (a, b) .

A particular value $z(a, b)$, computed at any fixed position (a, b) , is asymptotically standard Gaussian, if $N \rightarrow \infty$. But this convergence is not uniform: for a particular finite N , even a large one, the quantity $z(a, b)$ won't be Gaussian in some parts of the (a, b) plane. For example, points with too small scale a and points with b far outside of the sample range must be removed from the analysis, as done by the next step.

(iv) Applying a criterion of Gaussianity on z , we determine the admissible work domain \mathcal{D} in the (a, b) -plane. The simplest version of such a criterion is to have many enough sample objects x_i that contribute in \tilde{Y} with a significant amount. This requirement can be formalized as:

$$n(a, b) = \sum_{i=1}^N \varphi\left(\frac{x_i-b}{a}\right) \Big/ \int_{-\infty}^{+\infty} \varphi(t) dt \geq n_{\min}. \quad (3)$$

The criterion guarantees that the distribution of $z(a, b)$ remains almost Gaussian and does not degenerate inside \mathcal{D} . However, more subtle Gaussianity criteria should be used in practice, and they are given in (Baluev 2017).

Larger samples imply larger N , causing \mathcal{D} to expand to smaller scales a , while reducing N causes \mathcal{D} to shrink. Practical calculations revealed that for $N \lesssim 100$ the domain \mathcal{D} becomes (almost) empty, so our pipeline is useful mainly for $N \gtrsim 100$.

(v) Inside the work domain \mathcal{D} , we compute the maximum of $|z(a, b)|$. If this maximum is large enough, than there are significant deviations between the model Y_0 and the actual estimate \tilde{Y} . The formal significance threshold can be estimated via the false alarm probability (FAP) using an analytic formula, which is based on the assumption that $z(a, b)$ is Gaussian:

$$\text{FAP}(z) \simeq 2W_{00} z e^{-z^2/2}, \quad (4)$$

where the coefficient W_{00} can be determined simultaneously with the computation of \tilde{Y} and other quantities.

Setting some small threshold FAP_* , e.g. 0.01, and comparing the actual “observed” $\text{FAP}(z_{\max})$ with it, we can suppress the level of false detections to the desired low probability.

(vi) In practice, there are usually multiple places in the (a, b) plane, where $|z(a, b)|$ rises above the significance threshold. Their location indicate the shift and scale characteristics of the structures that we need to add to Y_0 to obtain a more matching model. Performing such a thresholding, i.e. selecting (a, b) points that satisfy $\text{FAP}(z(a, b)) < \text{FAP}_*$, we purge the noise from the (a, b) plane, and leave only significant structures.

(vii) After the noise thresholding, we can apply a generalized inversion formula

$$f(x) = \frac{1}{C_{\psi\gamma}} \int_{-\infty}^{+\infty} \int_{-\infty}^{+\infty} Y(a, b) \gamma\left(\frac{x-b}{a}\right) \frac{dad b}{|a|^3},$$

to the thresholded estimate $\tilde{Y}(a, b)$. Here, the optimal kernel γ depends on the adopted wavelet ψ , and they both define the normalization constant $C_{\psi\gamma}$. The inversion gives us an updated (or improved) comparison model Y_0 that includes

all the significant structures detected at the current iteration.

(viii) The steps (iii) and (v)-(vii) are cycled over, until we remove all the significant structures from the (a, b) plane (i.e., until $|z(a, b)|$ is suppressed below the significance threshold everywhere in \mathcal{D}). In the end we obtain a reconstructed p.d.f. estimate $\hat{f}(x)$ that contains only details that overpassed the desired level of significance. In the process, we also obtain information about the FAPs for the particular details detected.

At a glance, the pipeline involves three big blocks algorithmically interleaved:

- (i) estimation of the wavelet transform and related stuff;
- (ii) detecting significant structures;
- (iii) iterative reconstruction of the p.d.f.

We note that the last one, the reconstruction of the p.d.f., represents a version of the matching pursuit method. From this point of view it becomes similar to the famous CLEAN (Roberts et al. 1987) and CLEANest (Foster 1995, 1996) algorithms of the spectral deconvolution, which are also related to the matching pursuit (Hara et al. 2017).

In the most basic words, the matching pursuit is aimed to seek a “sparse” (that is, a constructively compact) approximation to some raw data. It offers an easy and a quick solution, but not necessarily the accurate one. In particular, in the time-series analysis by CLEAN/CLEANest there are difficulties with treating the aliases. A similar problem, appearing due to an “interferention” of the wavelets side lobes was revealed in this work too, although it did not become that important.

In practice, the problem appears when e.g. two structures approach each other closely. In such a case, the reconstructed p.d.f. $f(x)$ may contain an artifact between them that does not appear significant in the wavelet transform (in $z(a, b)$). Due to this effect, we stick a rule: consider the reconstructed $f(x)$ as just a useful hint that helps to intuitively interpret the 2D wavelet map, but we must refer to only $z(a, b)$ if it comes to the significance estimate of any pattern. In other words, if we see some interesting structure in the reconstructed p.d.f., this does not yet guarantee in itself that this structure is significant indeed. We must get back to the (a, b) plane and verify if the detail was indeed significant there.

Considering other works, probably the closest wavelet analysis method was provided by Skuljan et al. (1999). Let us list the main differences of our method from that one.

(i) We avoid any binning of the data. The binning is an unnecessary and possibly intervening procedure in this task. The sample is analysed “as is”.

(ii) We consider more general formulations in many aspects: use of a general comparison model, of two distinct wavelets, and paying attention to both positive and negative values of the CWT. This enables us to detect a variety of distribution patterns. Skuljan et al. (1999) use zero comparison model, only the MHAT wavelet, and consider only positive deviations, limiting themselves to only the clumps detection.

(iii) Our analysis relies on a normalized statistic that allows to equilibrate the noise over the shift-scale plane.

(iv) We corrected the significance testing approach to

adequately treat the effect of the “domain penalty”. We compute the false alarm probability (FAP) based on the CWT *extreme values* within a work domain. Skuljan et al. (1999) assumed wrongly a *single-value* distribution, triggering hidden multiple comparisons and p-hacking in the final result. This effect is analogous to e.g. the well-known “bandwidth penalty” in the periodogram analysis (Schwarzenberg-Czerny 1998; Baluev 2008; Süveges 2014), and it has a huge effect on the significance. Without taking it into account, the significance of a detection is dramatically overestimated, leading us to falsely confident conclusions.

(v) The FAP is approximated in a completely analytic way, thus removing any need of Monte Carlo simulations to estimate the significance.

(vi) Our method utilizes an objective criterion to determine the useful work domain in the shift-scale plane.

(vii) We apply optimal wavelets that allow to improve the S/N ratio and to increase the admissible work domain. In particular, the MHAT wavelet is basically useless in this task, because of the large non-Gaussianity it generates (Baluev 2017).

(viii) We built an optimized reconstruction kernel that allows to recover the p.d.f. from a “cleaned” CWT in a minimum-noise way.

(ix) The main limitation of our algorithm is that it can process only 1D distributions. It cannot analyse 2D distributions that were the main goal in (Skuljan et al. 1999), or distributions of higher dimension.

4 CONSTRUCTING EXOPLANETARY SAMPLES TO BE ANALYSED

We mainly utilize the public database available in the Extrasolar planets catalog (Roques & Schneider 1995). This database currently includes information and data about more than ~ 3000 exoplanets. However, this big ensemble appears too heterogeneous and needs to be split into several subsamples before performing any processing.

Since our analysis does not currently consider any formal treatment of the detection bias, we organize exoplanetary samples on the basis of their detection method. We construct two big subsamples: (i) planets detected by radial velocities, and (ii) planets detected by transits. These subsamples are not completely homogeneous yet, because they mix exoplanets discovered either in distinct Doppler or distinct transit surveys that differ in their accuracy and time base. This implies some differences in the corresponding “detection windows” that overlap with each other in a complicated way. We should bear this in mind, although it is unlikely that such a mixing effect would distort *small-scale* distribution details.

Our method can currently handle only single-dimensional distributions, and this implies further complications. There are multiple parameters associated to an exoplanet, and different parameters reveal correlations forming complicatedly shaped structures in the multidimensional space. Considering just single-dimensional distributions would mean to look at 1D projections of these structures. This infers information losses, in particular a decrease in sharpness. To suppress this effect to a certain degree at least, we can deal with various slices of the parametric space.

Table 1. Basic exoplanetary samples used in the work.

sample id	N	description
rv	708	Planets detected by radial velocity
rv.FGK	468	As above, but FGK stars only ($M_* \in [0.6, 1.4]M_\odot$)
rv.FGK.hmass	373	As above, but only giant planets ($m \sin i \geq 0.3M_{\text{Jup}}$)
pt	2730	Planets detected by primary transit
pt.FGK	2193	As above, but FGK stars only ($M_* \in [0.6, 1.4]M_\odot$)
pt.CKS	737	California Kepler Survey sample cleaned similarly to (Fulton et al. 2017), see Sect. 5.2.

We construct them by cutting the full exoplanetary sample with respect to some crucial parameters. These ‘cut parameters’ are different from the ‘target parameter’ that defines what distribution is investigated.

Simultaneously, we should take care about the sizes of the resulting samples when manipulating with them. In practice it appeared that samples smaller than 100 objects are useless in the analysis, because entire or almost entire shift-scale plane becomes non-Gaussian. Moreover, at least 300 objects are needed to obtain some informative non-trivial results.

Our main samples that we used in the analysis, are listed in Table 1. Note that some values were missed for some planets in the database, so when considering the distribution of particular parameters, the actual sample size can appear smaller than shown in the table.

We did not limit ourself to just drawing data from *The Extrasolar Planets Encyclopaedia*. Additionally we tried to reproduce the California Kepler Survey (CKS) sample that was used by Fulton et al. (2017) in their analysis of exoplanetary radii distribution. Using the data from (Petigura et al. 2017; Johnson et al. 2017), we followed the same steps: removed known false positives, removed stars with $K_p > 14.2$, put the constraints on the orbital period $P < 100$ d and on the impact parameter $b < 0.7$, removed giant stars using the same criterion as in (Fulton et al. 2017), and limited the temperature range by 4700 – 6500 K.

Unfortunately, we failed to reproduce the final sample precisely. The most problematic stage was filtering $b < 0.7$. The cited works lack the values for b and do not mention where they taken from, so we decided to extract b from the NASA Exoplanet Archive (NASA 2017). It appeared, however, that the final sample shrunked to $N \sim 700$, which is smaller than $N \sim 900$ in Fulton et al. (2017). We therefore decided that these values of b from the NASA archive might be less trustable, and then softened the threshold a bit, $b < 0.8$. But to compensate for an increased fraction of possibly unreliable radii estimates, we added an extra constraint that the relative uncertainty in the planet radius must be below 0.1. Thus we had $N = 737$ planet candidates left in the sample.

5 RESULTS OF THE ANALYSIS

In this section we present results of the analysis for various 1D distributions of exoplanets. We show numerous figures below, corresponding to different samples and distributions of different quantities. Before we proceed, some words must be said about how to interpret these plots.

All figures follow the same layout. We provide 4 graphs for each distribution analysed.

The *top pair* in each quartet demonstrates wavelet transforms estimates for the CBHAT and WAVE2 wavelets, or speaking more carefully, the significance colormaps for $z(a, b)$ for these wavelets.

The colormaps are computed assuming the comparison model $Y_0 = 0$, i.e. they correspond to the starting iteration of the matching pursuit algorithm. Everything that appeared significant in these maps, necessarily contributes to the corresponding reconstructed p.d.f.

For each point in the (a, b) plane, the value of $z(a, b)$ is computed, and then the FAP is calculated according to (4). However, we found it more intuitive to plot not this FAP itself, but its corresponding Gaussian quantile:

$$g = \Phi^{-1} \left(1 - \frac{\text{FAP}}{2} \right), \quad (5)$$

where Φ is the cumulative function of the standard normal distribution. Thus, g represents the absolute deviation that a standard Gaussian random variable can achieve with probability $1 - \text{FAP}$, so that the probability to fall out of the $\pm g$ range is equal to FAP. In other words, the quantity g is a classic normal significance level, or what is often called the “ g -sigma” significance. This quantity $g(\text{FAP}(z(a, b)))$ is plotted under the name “EVD significance level” (with EVD standing for the Extreme Value Distribution).

The significance color is panted only inside the normality domain \mathcal{D} , and everything outside of \mathcal{D} is hashed out. For the sake of comparison and extra validation, we additionally plot the simplified normality criterion (3) as a thick black curve. Usually, this curve traces rather well the lower boundary of \mathcal{D} , although local but important differences may appear sometimes.

In the *bottom pair* of graphs in each quartet, we show a histogram of the corresponding sample and the reconstructed p.d.f. for three significance levels, $g = 1$ (green), $g = 2$ (cyan), $g = 3$ (yellow). These three curves differ only in color, because even in the grayscale plot it remains always obvious, which one is which (larger smoothness means larger g).

We need to make a couple of final notes.

Whenever some feature is detected in the $z(a, b)$ graph and barely achieves e.g. $g = 2$ at its maximum, it will be *purged completely* in the corresponding p.d.f. plot (also for $g = 2$). Paradoxically, a two-sigma detail should normally disappear on the two-sigma p.d.f. curve. It could be seen only in the one-sigma p.d.f. curve, while to appear at the $g = 2$ curve, a pattern must rise *above* $g = 2$ in the colormap. Moreover, even if a feature does rise above the selected g -level in the colormap, it may appear practically invisible in the p.d.f. reconstruction just because it is small in absolute magnitude (regardless of the high significance). This is a normal behaviour that should not puzzle the reader.

From the other side, an opposite effect may appear sometimes. It was already mentioned in the previous section,

that when two or more features are located closely, they may interfere with each other in the reconstructed p.d.f. This effect may possibly generate new features in the p.d.f. graph, even if they were not present (or were not significant) in the wavelet transform. We reiterate again that currently our reconstructed p.d.f. curves should be treated just as an auxiliary visual tool. They do not provide reliable significance information. The significance of any structure must be derived from the $z(a, b)$ and its corresponding g -levels plots, while the p.d.f. plot just helps us to understand, how these structures may look.

5.1 Orbital periods and semimajor axes: fine-structured iceline accumulation?

Results for the period and semimajor axis distributions (both in logarithmic scale) are shown in Fig. 1 and 2. They refer to the *rv.FGK* subsample. It is well-known that these distributions should behave similarly, thanks to the third Kepler law, so we consider them here together.

First of all, we can see the large-scale structure: a highly-populated wide peak of long-period “warm jupiters”, a shallow concentration of “hot jupiters” at short periods, and a wide “period valley” between them. These are well-known features, more or less successfully explained by contemporary simulation works on planet formation and migration, see e.g. [Ida & Lin \(2004, 2008\)](#) and many more.

In particular, the predominant WJ maximum is attributed to the effect of the so-called iceline accumulation. It was explained in ([Ida & Lin 2008](#)) and extensively studied in many works after (e.g. [Schlaufman et al. 2009](#); [Hasegawa & Pudritz 2013](#)). Near the snow line physical processes of ice particles migration, evaporation, outward diffusion and recondensation interact so that the density of the material increases. This favours to planet formation just beyond the ice line. Moreover, if a protoplanet grows to form a giant planet (above Saturn or Jupiter mass), it then migrates modestly, so that the corresponding concentration of giant planets gets shifted inward.

The inner boundary of the WJ family corresponds to the semimajor axis $A \sim 1$ AU or orbital period $P \sim 300$ d.¹

In Fig. 1-2 we can also see a fine-structured pattern, in the period distribution especially. It appears as a smaller-scale local maximum layered over the large-scale one, close to the upper boundary of the PV depression. In the reconstructed p.d.f. curves this substructure looks like an overshoot peak, maybe even causing a bimodality. However, we must be careful with these curves due to possible artifacts of the matching pursuit. To gain more accurate understanding of what actually happens there, we must refer to the corresponding wavelet transforms.

Let us focus on the period distribution at first, Fig. 1.

In its CBHAT wavelet transform, we can see a remarkable negative (cyan) spot at $P \sim 450$ d, with a relatively small scale $a \sim 0.3$.² It reaches 3-sigma level that confirms

its high significance. Such a spot indicates that the p.d.f. attains a high curvature at this location (with upward convexity). This does not necessarily indicate a local maximum, but at least a zone of relatively abrupt transition between the PV and WJ domains.

Such an abrupt transition is confirmed by the WAVE2 transform, where we can see a high-significance domain near $P \sim 350$ d that descends to the same small scales.

All this suggests the following interpretation concerning the log P distribution of the *rv.FGK* sample:

- (i) there is a quick density gradient near $P \sim 350$ d, corresponding to the PV/WJ boundary;
- (ii) this gradient ends with a highly-curved p.d.f. convexity near $P \sim 450$ d that further turns into the wide maximum of long-period planets.

At this stage we still cannot say, if there is indeed an additional local maximum at $P \sim 450$ d or any separated subfamily of exoplanets.

To ensure that we talk about a subfamily, we would need to detect some side *separations* from the remaining planets. That is, the small-scale spot at $P \sim 450$ d in the CBHAT wavelet map should be accompanied by a couple of counter-signed spots on both sides. They would indicate concave zones in the p.d.f., meaning that the central convexity represents a standalone formation.³

In fact, we do note some secondary spot in Fig. 1, but unfortunately its significance is too small, below $g = 2$.

Now we can use theoretic results to decide what sample to analyse further. Simulations of the iceline barrier effect from e.g. ([Ida & Lin 2008](#)) predict that in the range of interest, $P \sim 300 - 1000$ d, less massive planets would only represent an interfering background that blurs the giant planets subsample. The positions for the “Warm Jupiters” and “Warm Neptunes” maxima should be displaced considerably, because their migration histories are different. Therefore, it might be reasonable to analyse the subsample of giant planets, *rv.FGK.hmass*. This subsample should reveal the iceline accumulation effect in a more clean manner.

These results are presented in Fig. 3-4. We can see that all the fine-scale structures within the range $P \sim 300 - 1000$ d indeed gained more magnitude. In the CBHAT wavelet transform, we can see the primary (negative) spot at $P \sim 450$ d that got the significance $g = 3.4$, accompanied by a pair of the counter-signed secondary spots at $P \sim 700$ with $g = 2.1$, and at $P \sim 250$ d with $g = 2.0$. Such a triplet pattern highlights a statistically separated narrow subfamily of giant planets in the period range $\sim 300 - 600$ d. In the p.d.f. graph it looks like an overshooting peak right after an upturn.

This significance increase was achieved by restricting the exoplanetary sample from *rv.FGK* to *rv.FGK.hmass*, but this is not a p-hacking or data-driven analysis. It would be those, if we just searched many subsamples in the hope to finally obtain a desired significant result. But our decision of how to restrict the sample relied on the previous

¹ The notation A for the semimajor axis should not be mixed with a standing for the wavelet scale.

² Since we analyse the distribution of log P actually, a has the meaning of a relative scale. That is, $a = 0.3$ infers about ± 15 per cent range from a given P .

³ When saying *separation*, we mean a concavity, not a local minimum. But these patterns are basically equivalent, because they can turn one into another after adding a larger-scale background gradient.

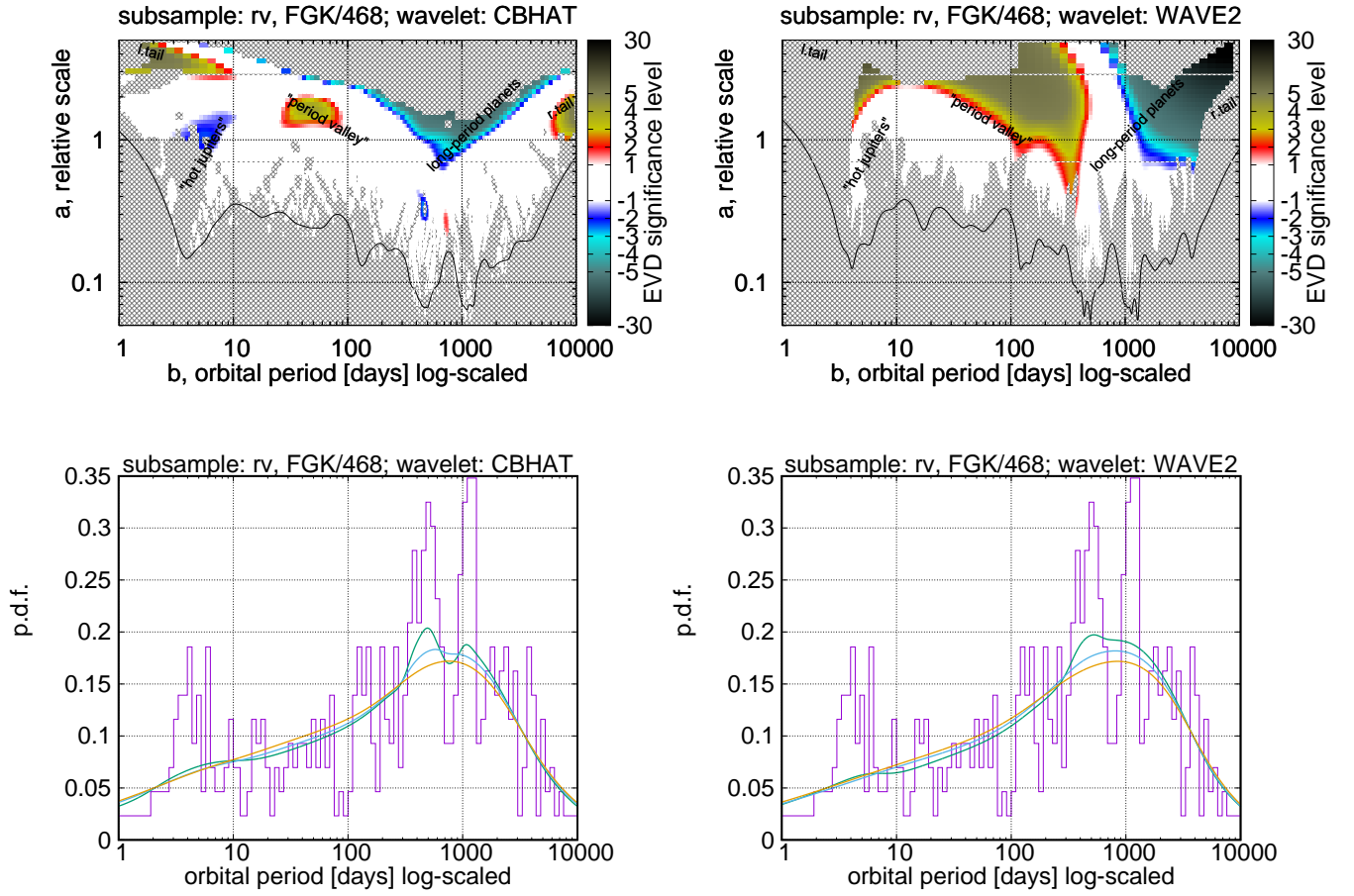


Figure 1. Subsample: RV detection method, FGK-type host stars, $N = 468$. Variable: orbital period.

theoretic knowledge, regardless of any statistical analysis already done. The second sample could equally decrease the significance of the result rather than increase it. In such a case, this subsequent analysis attempt does provide additional evidence.

In either case, there is no significant hints of bimodality within the WJ maximum. Although some of the p.d.f. plots, e.g. in Fig. 3, suggest bimodality, it looks like a reconstruction artifact appearing due to inherent weaknesses of the matching pursuit algorithm.

So far we considered only the period distribution, but orbital semimajor axes are apparently more appropriate concerning the iceline barrier effect. Disappointedly, this distribution does not reveal so much subtle details (Fig. 2.4). With the CBHAT wavelet, we can see just a single small-scale spot at $A \sim 1.1$ AU indicating a local convexity. In the subsample of giant exoplanets, its significance barely reaches the two-sigma level, and it becomes even worse in the larger *rv.FGK* sample.

The semimajor axis A is merely a derived parameter, while the primary “observed” quantity is the orbital period P . Knowing P , we can recover A using the third Kepler law:

$$P \propto M_{\star}^{-\frac{1}{2}} A^{\frac{3}{2}}, \quad A \propto M_{\star}^{\frac{1}{3}} P^{\frac{2}{3}}, \quad (6)$$

where M_{\star} is the star mass. However, the value of M_{\star} is

not the same for all exoplanets. In this case (6) defines a statistical correlation between P and A rather than a strict binding. That is, the P - and A -distributions should look generally similar, but small-scale details would be different due to the scatter in M_{\star} . If a detail appeared sharp in the P -distribution, it gets blurred in the A -distribution, and vice versa. It cannot remain sharp in the both.⁴

Our analysis revealed that small-scale subfamily discussed above appears sharply in P . But then it should necessarily fade out in A . Since this is a necessary and predictable behavior, it does not make the detection less reliable from the statistical point of view.

But then an interesting question emerges: should the iceline barrier effect generate more sharp details in a - or P -distribution? Unfortunately, simple considerations did not provide us with a definite answer. By combining (6) with the inverse-squares law, it is easy to assess the distance of the ice line, a_{ice} , and the corresponding Keplerian period, P_{ice} , as a function of the star luminosity:

$$L_{\star} A_{\text{ice}}^{-2} = \text{const} \implies A_{\text{ice}} \propto L_{\star}^{\frac{1}{2}}, \quad P_{\text{ice}} \propto M_{\star}^{-\frac{1}{2}} L_{\star}^{\frac{3}{4}}. \quad (7)$$

⁴ Note that details in the A -distribution should be always blurred additionally, because M_{\star} often involves remarkable uncertainties. But this effect is smaller than the scatter of M_{\star} in the sample.

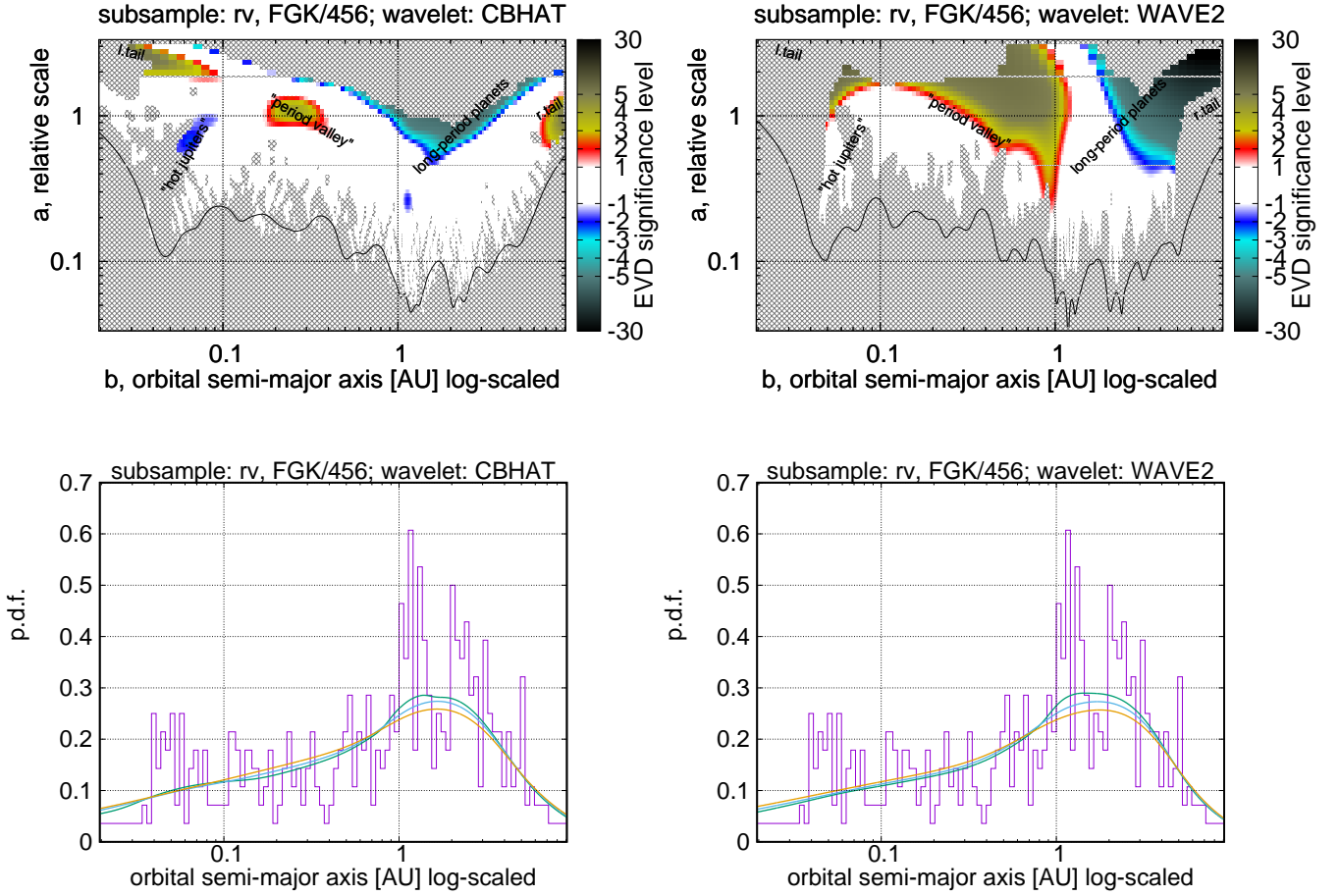


Figure 2. Subsample: RV detection method, FGK-type host stars, $N = 456$. Variable: orbital semimajor axis.

And by applying the mass-luminosity relation, $L_* \sim M_*^4$, we obtain

$$A_{\text{ice}} \sim M_*^2, \quad P_{\text{ice}} \sim M_*^{-\frac{5}{2}}. \quad (8)$$

But then it follows that *both* the A - and P -distributions should be blurred approximately equally, because A_{ice} and P_{ice} depend on M_* via almost the same power degree (2 or -2.5 , the sign does not matter).

However, the formulae (8) do not take into account the migration of planets. The migration rate and its distance should correlate with M_* somehow, but this correlation depends on multiple factors. It is difficult to predict without performing simulations like those available in (Ida & Lin 2008). Depending on the sign of the correlation, it may sharpen either of the two distributions. In principle, this can be used to verify the iceline nature of the exoplanetary subfamily for $P \sim 300 - 600$ d.

At last, we recall that the database of *The Extrasolar Planets Encyclopaedia* is heterogeneous, mixing planet candidates discovered by multiple independent Doppler programmes. Such mixed samples might demonstrate spurious effects due to an overlap of different detection thresholds. However, most radial-velocity surveys are very aged already, and they are pretty complete in the period range of 300–600 d (for giant planets at least). Moreover, the orbital

period P is one of the best-determined exoplanetary characteristics. It is therefore unlikely that observational selection, sample heterogeneity, or possibly inaccurate data could cause any unusual statistics in this period range.

5.2 Transiting planets radii: confirming evaporation valley

The radii distribution among Kepler exoplanetary candidates demonstrates signs of a bimodality (Fulton et al. 2017). There are two local maxima of the density at $R = 1.3R_{\oplus}$ and $R = 2.4R_{\oplus}$, while planets with R in the intermediate range $1.5 - 2.0R_{\oplus}$ are comparatively rare. This effect was named the “evaporation valley”, and it has got a detailed theoretic treatment already (Owen & Wu 2017). In a few words, higher-mass planets are capable to preserve their dense atmospheres even if they are exposed to intense irradiation from the star, but low-mass planets loose most of their atmospheres eventually, reducing their sizes to even smaller values than they initially were.

We were interested to apply our algorithm to this case. First of all, we followed our common protocol set in advance, i.e. we analysed the transit sample *pt.FGK*, drawn from the database of *The Extrasolar Planets Encyclopaedia*.

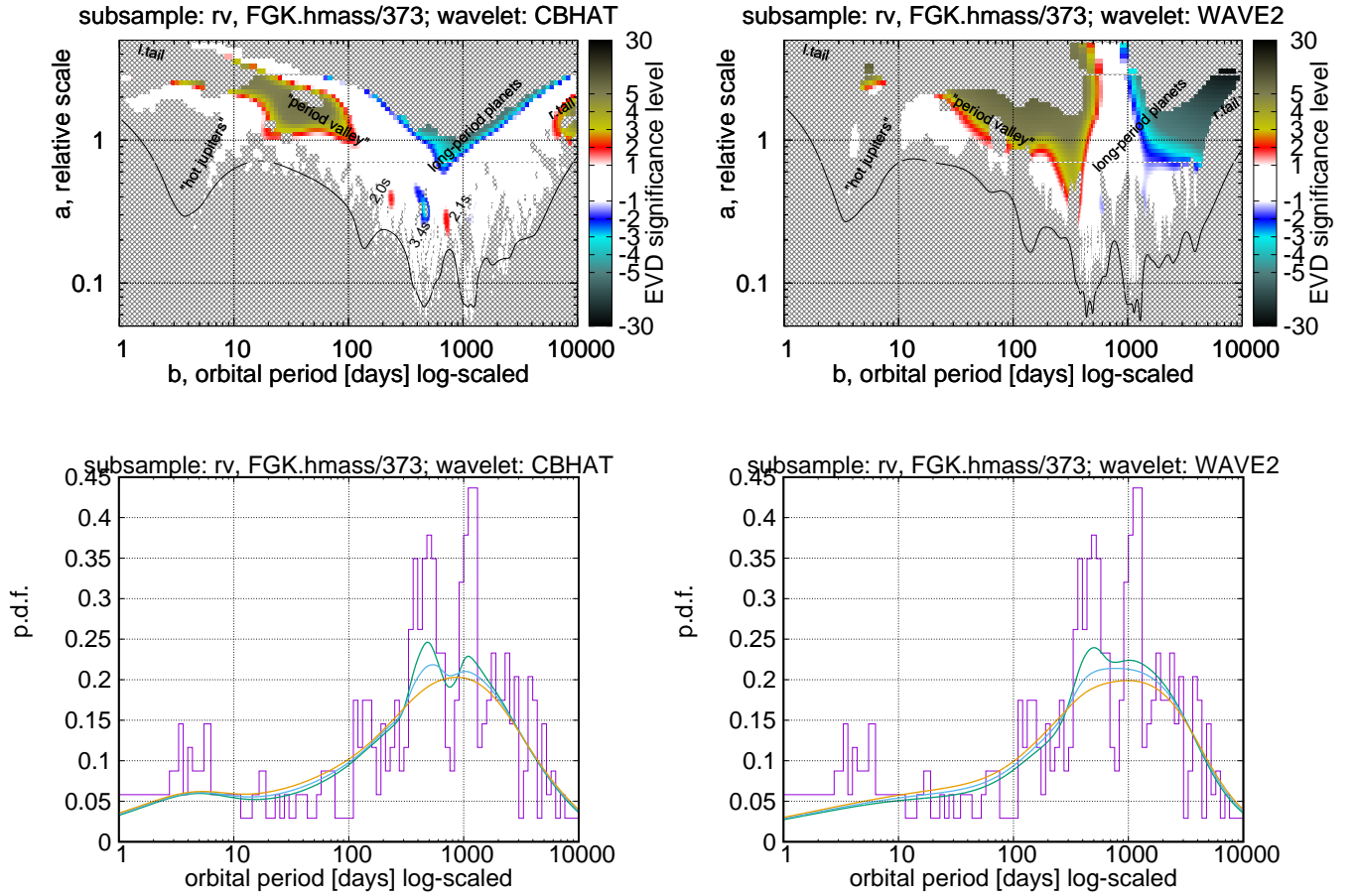


Figure 3. Subsample: RV detection method, FGK-type host stars, higher-mass planets ($m \sin i > 0.3M_{\text{Jup}}$), $N = 373$. Variable: orbital period. Fine-scale structures are labelled with the significance quantile g (the number of Gaussian “sigmas”).

This sample includes Kepler candidates, as well as those detected by more common but less sensitive ground-based surveys. The results for the planet radii distribution are shown in Fig. 5.

A bimodality is obvious in the reconstructed p.d.f., though this is unrelated to the “evaporation valley”. The peaks are for the families of giant Jupiter-sized planets and of the Earth-/super-earth-sized ones. They are separated by a wide minimum in the range $0.4 - 0.8R_{\text{Jup}}$. These major families with an intermediate desert are undoubtful, and were predicted quite early, at least by [Ida & Lin \(2004\)](#).

Apparently nothing related to the “evaporation valley” can be spotted in this p.d.f., but we can see in the CBHAT wavelet transform a small negative (blue) spot located at $R \sim 0.12R_{\text{Jup}}$ or $1.3R_{\oplus}$. It represents a hint of a smaller-scale p.d.f. convexity. Its significance is above two-sigma, but the absolute magnitude appears so small that practically nothing can be seen in the reconstructed p.d.f., or even in the histogram, at this location.

In the WAVE2 wavelet transform there is a fancy anomaly at $R = 0.2R_{\text{Jup}}$ and $a = 0.2 - 0.3$, indicating a relatively more quick uprise density gradient at this location. Although, in the reconstructed p.d.f. it does not appear obvious too.

Likely, these subtle hints is all what is left from the “evaporation valley” in this sample. The database in ([Roques & Schneider 1995](#)) is extremely heterogeneous for transiting planets. And contrary to the previous subsection, we are now interested in the range where many surveys appear incomplete. Transit programmes have different detection limits, and their selection functions get overlaid, imposing spurious distortions to the statistics. Besides, it seems that this catalog is quite “dirty” with respect to false positives and unreliable values. It is not very much surprising that the “evaporation valley” could not be reliably reproduced with these data, although our method was able to detect some remaining hints.

After that, we applied our analysis to the more homogeneous CKS data cleaned as described in Sect. 4. The results are shown in Fig. 6. Now we can clearly see a bimodal radii distribution with maxima at $1.3R_{\oplus}$ and $2.6R_{\oplus}$, and a gap between them. Though our sample is not strictly the same as in ([Fulton et al. 2017](#)), the histogram does not reveal any obvious visual difference.

But contrary to [Fulton et al. \(2017\)](#), our analysis does not provide so strong statistical support to the bimodality. Although the CBHAT wavelet clearly reveals a pair of convexity zones at 1.3 and $2.4R_{\oplus}$, the concavity between them

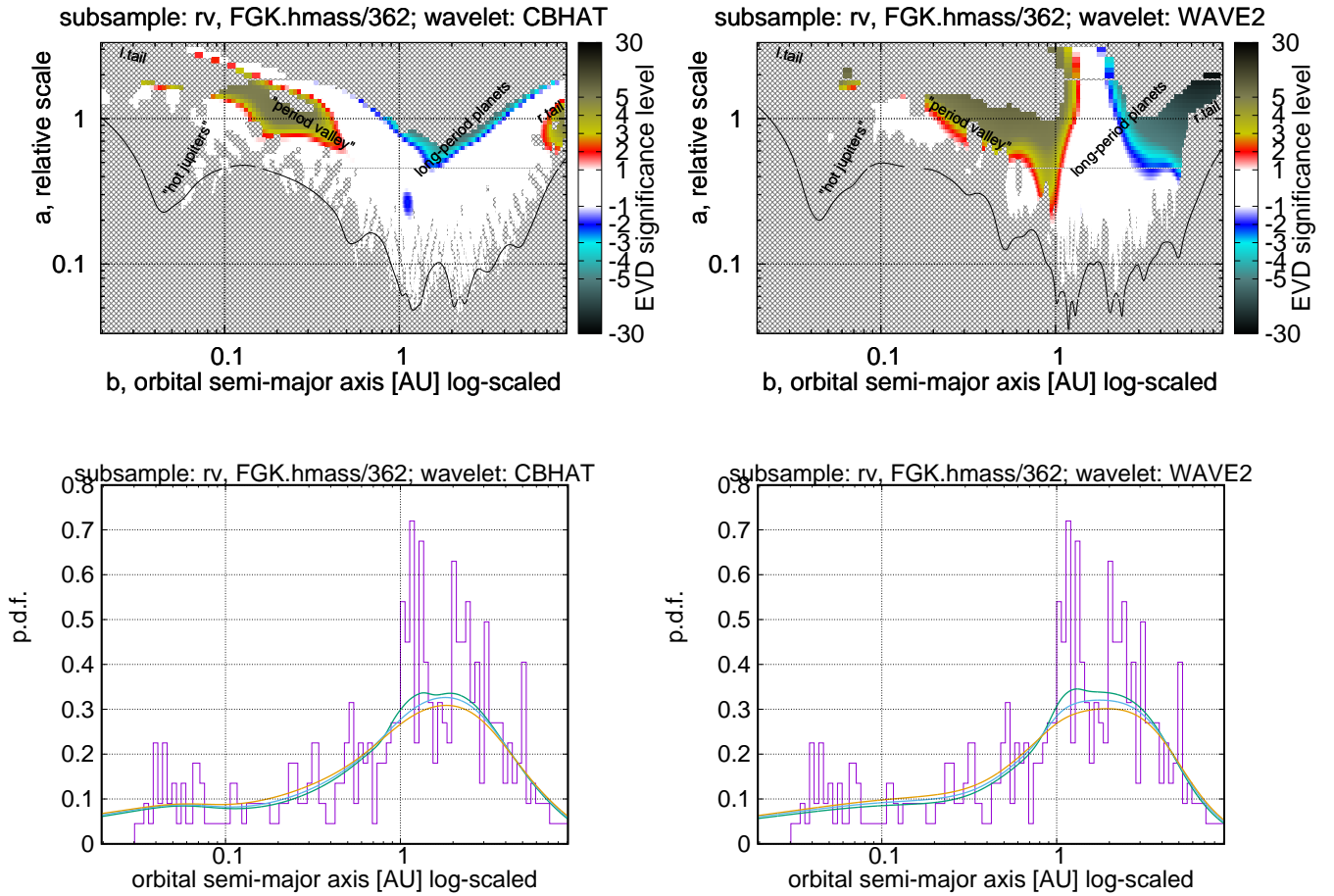


Figure 4. Subsample: RV detection method, FGK-type host stars, higher-mass planets ($m \sin i > 0.3M_{\text{Jup}}$), $N = 362$. Variable: semimajor axis.

does not reach enough significance. The convexities are undoubted, but on themselves they do not yet tell anything in support of the bimodality and do not confirm standalone exoplanetary families. Without a clear intermediate gap, the density function may have just a plateau-like shape with more abrupt sides. That would mean just a single density maximum without any subfamilies.

Ensuring the bimodality necessarily requires to detect a gap, or at least an intermediate concavity. However, this feature does not appear statistically significant with the CBHAT wavelet (only $g = 1.5$). A concavity and even a local minimum is obvious in the reconstructed p.d.f. even for $g = 3$, but this looks like an artifact of the matching pursuit algorithm, since such a significance level is not supported by the wavelet transform. So, the CBHAT wavelet fails to detect the “evaporation valley”.

The WAVE2 transform in Fig. 6 appears a bit more promising: it resolves a dipole-like standalone pair of descent/uprise patterns, and the uprise portion at $R = 2R_{\oplus}$ appears moderately significant, $g = 2$.

Being puzzled by such an inconsistency with [Fulton et al. \(2017\)](#), we investigated the argumentation from that work.

(i) *Non-parametric Kolmogorov–Smirnov and Anderson–Darling tests to verify the agreement with a loguniform distribution.* Even if the R -distribution does deviate from the loguniform one significantly, this conclusion tells us nothing in favour of possible bimodality. There are many unimodal distributions that could be different from the loguniform one. The K–S and A–D tests are just unable to provide any information concerning multimodality. They are irrelevant to the task at all.

Besides, the application of those tests is clearly illegal, because the loguniform model is incomplete. The left and right cutoff positions were unknown to the authors *a priori* and were guessed from the same data.

(ii) *The dip test of unimodality by Hartigan & Hartigan (1985).* The test is well-known and useful in itself, but its application nonetheless seems invalid due to a hidden pre-analysis. It is likely that the authors decided to apply this particular very specific test only because the bimodality was initially suspected by visual inspection of the histogram for the same Kepler data. If the data were different then such a suspicion would not appear, and the question of bimodality would not arise at all. In such a case, some other peculiarity could be spotted, triggering the use of another specific test designed to detect patterns of that type. Again, we can

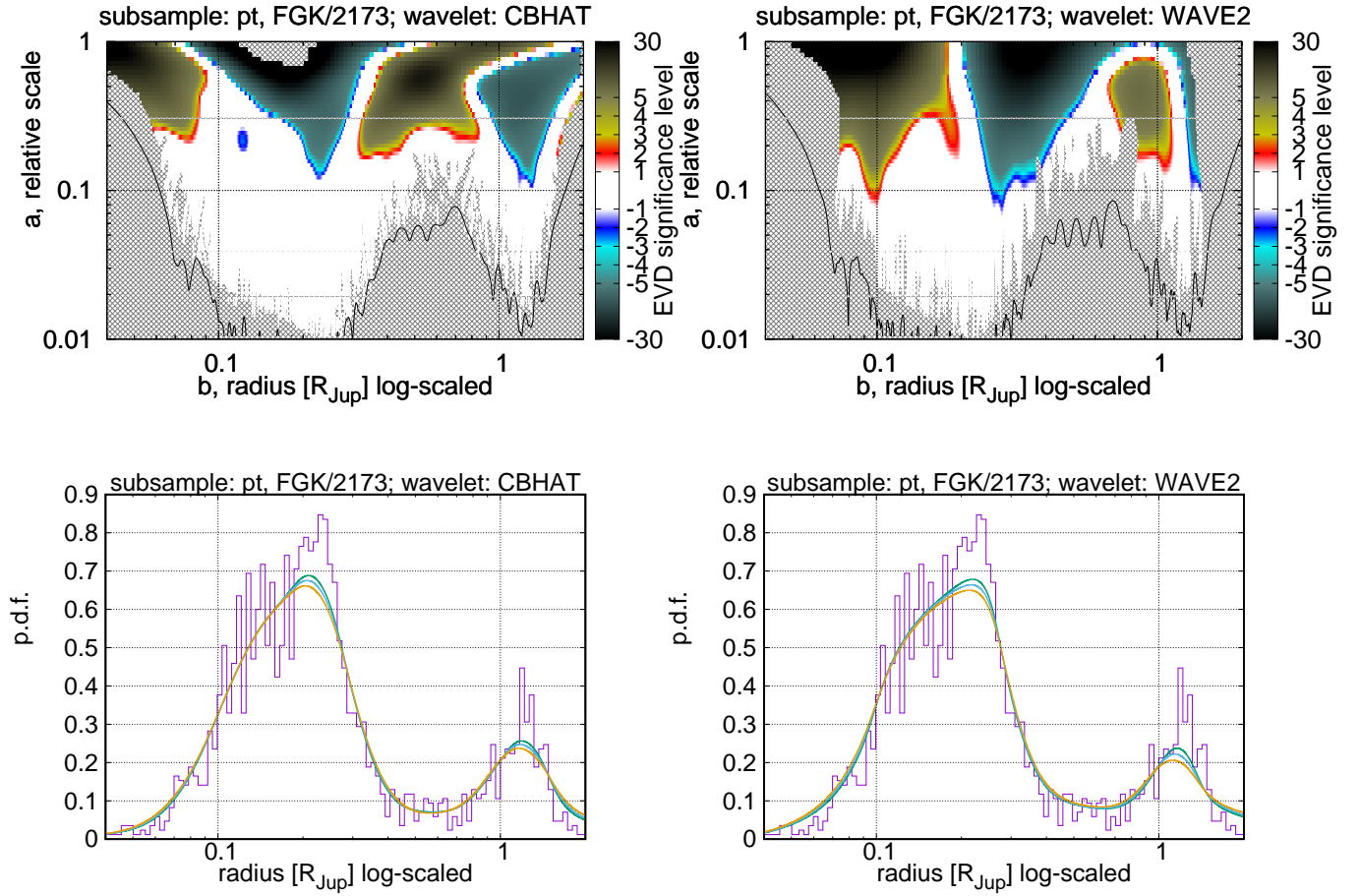


Figure 5. Subsample: Primary transit detection method, FGK-type host stars, $N = 2173$. Variable: planet radius.

clearly see a condition for a data-driven analysis: the hypothesis was formulated from the same data that were then tested as if this hypothesis was given in advance.

We nonetheless applied the [Hartigan & Hartigan \(1985\)](#) test to our version of the CKS sample to compare the results. We failed to reproduce the same high significance level as [Fulton et al. \(2017\)](#). Instead of $\text{FAP} = 0.14$ per cent (or $g = 3.2$), for the log R data we obtained merely $\text{FAP} = 3$ per cent or 2.2-sigma significance. If it is not a software bug in either work⁵ then the test itself might be not very robust. We considered other CKS subsamples, filtering the data at different levels of tolerance. The best significance from the dip test was $\text{FAP} = 0.6$ per cent, if we preserved the radii with uncertainties greater than 10 per cent. However, even this significance is much worse than [Fulton et al. \(2017\)](#) reported.

(iii) *Fitting a spline model and spline deconvolution.* The main conclusion was that because of a ~ 12 per cent uncertainty in the planet radii, the “observed” R -distribution is merely a smoothed version of the original, “underlying”,

distribution of the precise radii. Hence, the true distribution must have a deeper bimodality gap than it seems from the observation.

There is no doubts on this conclusion, but it does not offer us any additional evidence in favour of the bimodality, because it has nothing to do with the statistical significance. The true gap should be deeper only if it actually exists, i.e. if the observed one is not a noise artifact. Otherwise, the gap just does not exist in the both distributions.

The conclusion is that the hints of the gap in the radii distribution are not ignorable, but its significance remains rather marginal. Its reliability is much worse than [Fulton et al. \(2017\)](#) claimed. We definitely cannot give it any “strong support”. An optimistic significance estimate is about two-sigma level.

5.3 Orbital eccentricities

We treated the orbital eccentricity e as a symmetric parameter, extending its distribution to the negative range, $e \Leftrightarrow -e$. This was necessary to avoid an artificial distribution cutoff at $e = 0$, in order to process the low-eccentricity domain more adequately. To reach this goal, we duplicated every e

⁵ We used a public PYTHON implementation of the test, available at <https://github.com/alimuldal/diptest>.

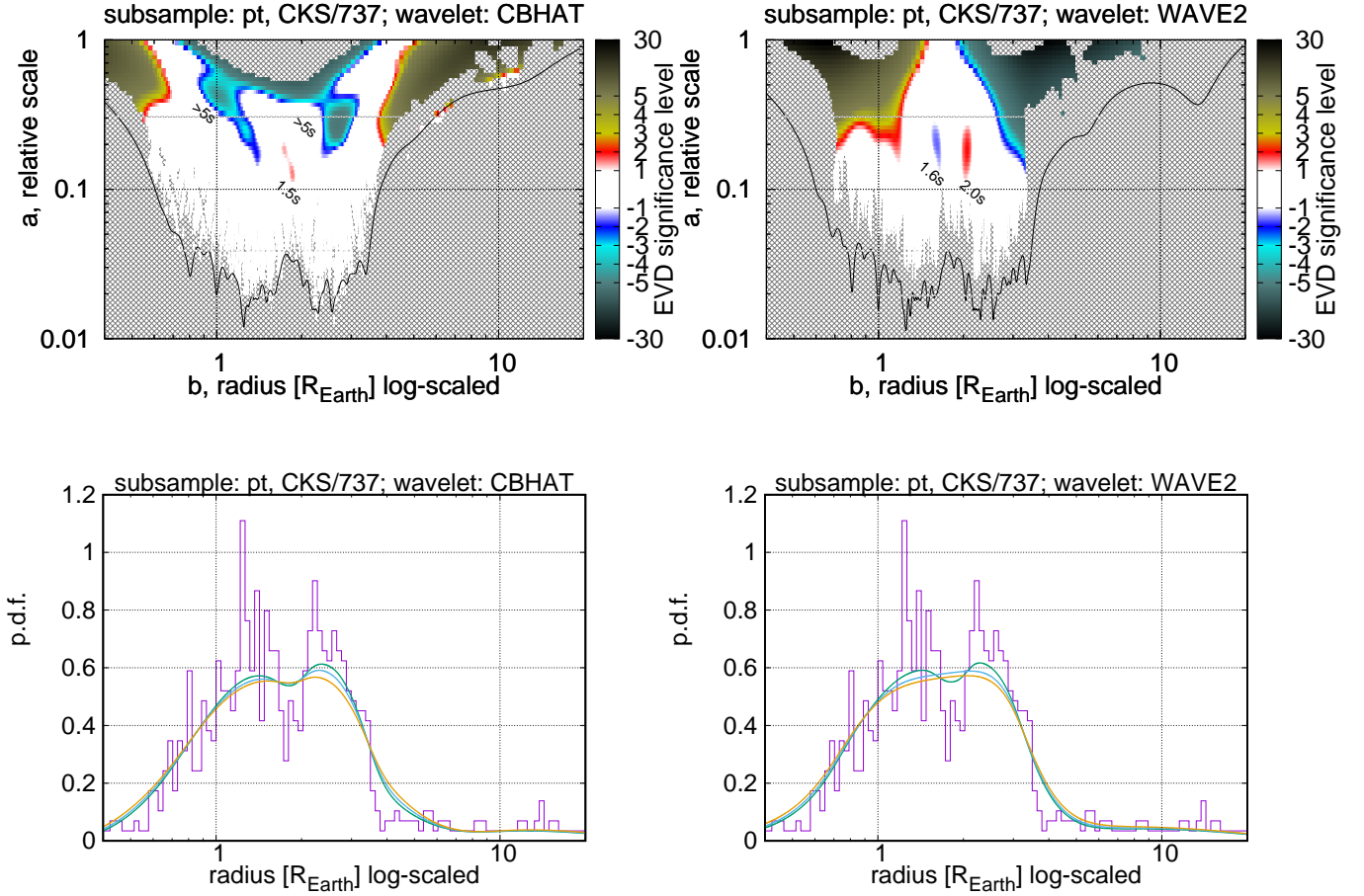


Figure 6. Subsample: California Kepler Sample (CKS) with filters (see text), $N = 737$. Variable: planet radius. Fine-scale structures are labelled with the significance quantile g (the number of Gaussian “sigmas”).

value in the sample with $-e$. Thus we artificially increased the sample size to $2N$, but when computing the significance and related stuff, we substituted the correct size of just N , so that such a manipulation should not lead to an overestimated significance. Also, we consider our work domain \mathcal{D} only for $e \geq 0$, so the coefficients in the FAP estimate (4) do not get doubled (this would lead to an underestimated significance otherwise).

We recognize that even with such corrections the analysis might be not fully rigorous, because instead of the pure CBHAT and WAVE2 we basically use wavelets of a different shape, symmetrized about zero. The actual remaining effect is not obvious, but we did not try to treat it better, because we did not obtain any remarkable results with this distribution.

The results for the *rv.FGK* sample are presented in Fig. 7. We can see an intricate small-scale structure near $e = 0$ that consists of a very narrow peak accompanied by narrow side gaps. Such a structure near $e = 0$ is not surprising and it can be explained by the following obvious sources:

(i) Deficient RV data are usually fitted with the eccentricity fixed at zero. This leads to an increased height of the

$e = 0$ peak, because some exoplanets with non-zero e are reset to zero.

(ii) If the eccentricity is fitted, it is frequently biased to a larger value due to a non-linearity in the Keplerian RV model. This bias moves some exoplanets with small e away from zero, forming a gap about $e = 0$ that serves as a background for the central very narrow peak.

(iii) There is a well-known physical phenomenon of tidal circularization that settles many “hot jupiters” to $e \approx 0$, further increasing the central peak.

We can see that only the third effect is physical and related to the actual eccentricity distribution, while the other two are only apparent effects imposed by the RV data fitting.

We did not reveal any other small-scale structures in this distribution. Also, we did not analyse transit candidates here, since most of them do not have a good eccentricity estimate.

5.4 Orbital periastra: no hints of a detection bias

We analysed the distribution of the orbital pericenter argument, ω . Our motivation was to detect possible selection ef-

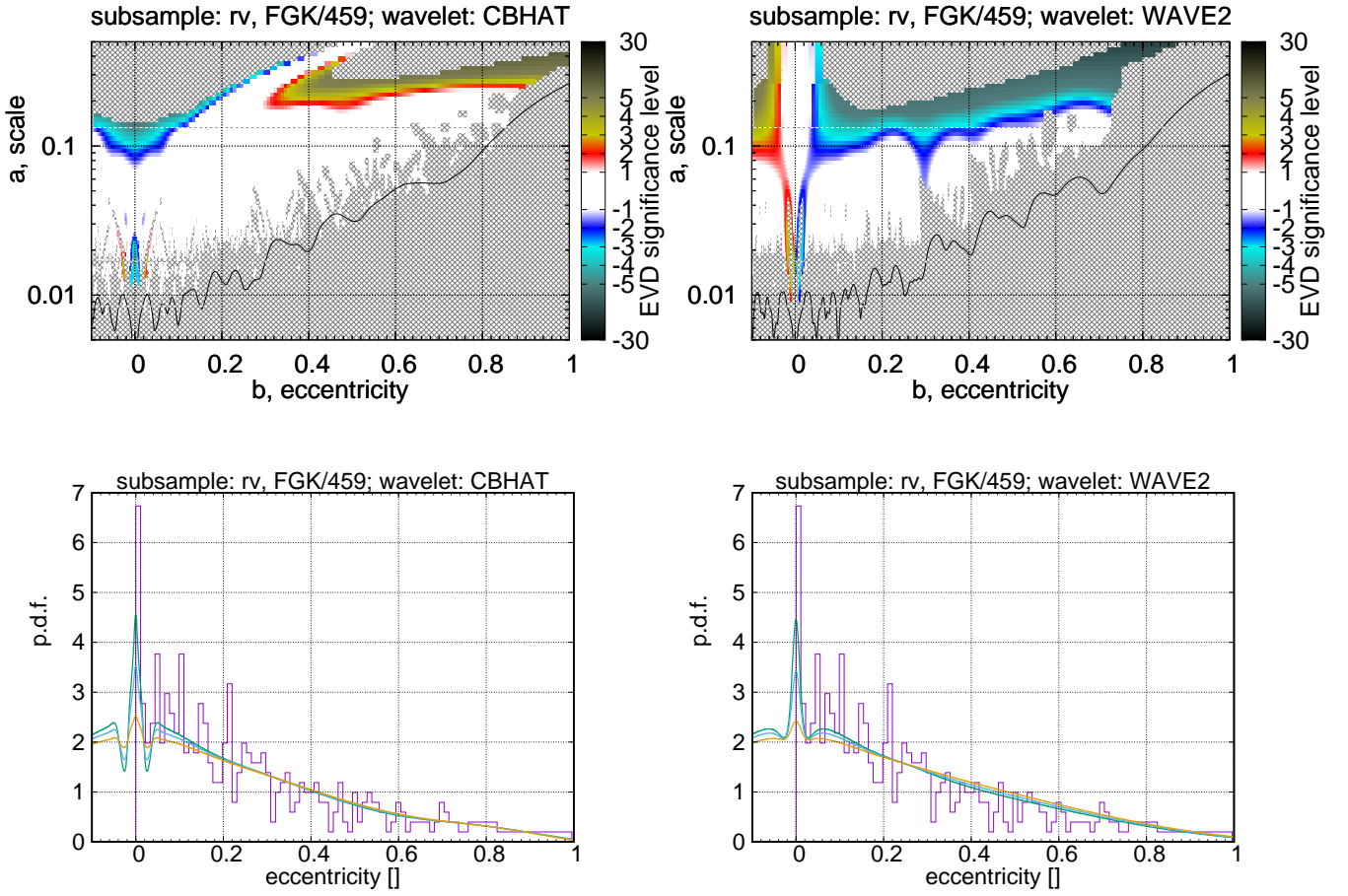


Figure 7. Subsample: RV detection method, FGK-type host stars, $N = 459$. Variable: orbital eccentricity.

fects. Any detection bias in e should reveal itself in the ω too, because the shape of the eccentric Keplerian RV curve depends on ω dramatically. In the eccentricities we cannot disentangle this bias from the actual distribution shape, which is unknown. However, the spatial orientation of exoplanetary orbital periastra should likely be isotropic, meaning a uniform distribution in ω . Therefore, any deviation from the uniform distribution would immediately indicate a detection bias.

The results for the ω -distribution (the rv sample) are presented in Fig. 8. Additionally to this full sample, we also computed wavelet maps for various subsamples by removing low-eccentric exoplanets ($e < 0.15, 0.20, 0.35$). In either case, the distribution is consistent with the uniform one. No significant deviation was detected.

Note that to avoid non-physical cutoffs at $\omega = 0$ and $\omega = 2\pi$, we applied an approach similar to that from Sect. 5.3: we replaced every sample value ω with a triplet $\omega - 2\pi, \omega, \omega + 2\pi$. This artificially increased the total sample size to $3N$, but we again used just N in the significance estimates where appropriate.

5.5 Planet masses

Finally, we present our results for the exoplanetary mass distribution. In this analysis, we considered the $rv.FGK$ and $pt.FGK$ samples. Note that the second (transit) sample appeared much smaller than e.g. transit sample in Sect. 5.2, because the planet mass can be determined only by radial velocities. Most transiting planet candidates remain unconfirmed by the Doppler method, mainly because of technical limitations on faint stars. As a result, both the samples appeared to have almost the same moderate size, $N \sim 500$.

The results are presented in Fig. 9 ($rv.FGK$ sample, distribution of $m \sin i$) and in Fig. 10 ($pt.FGK$ sample, distribution of m). In the first case, the distribution appears unimodal with a wide maximum covering the range $m \sin i = 0.5 - 5M_{Jup}$. On contrary, the transit sample reveals an undoubtful bimodality, with a secondary maximum at $m \sim 0.03M_{Jup}$ (or $\sim 10M_{\oplus}$). The first maximum involves giant exoplanets, while the second one incorporates super-earths and Neptune-mass planets. The gap between the families covers the range $m = 0.1 - 0.3M_{Jup}$.

We may conclude that the transit detection technique is remarkably more sensitive to low-mass planets. Although all exoplanets in the both samples were observed by the radial velocity technique, the transit candidates required just an

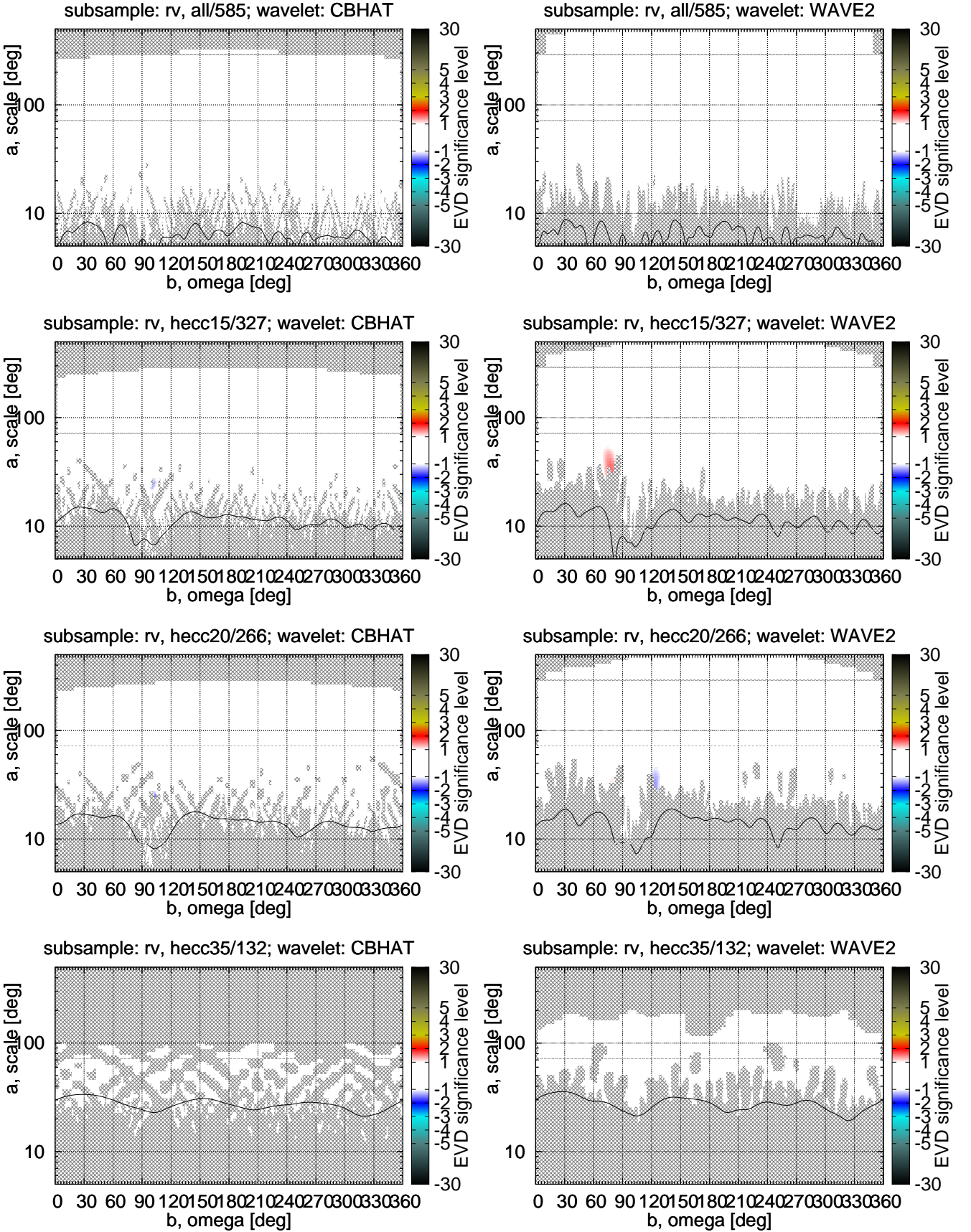


Figure 8. Subsample: RV detection method, cutting higher eccentricities ($e > 0.15$, $e > 0.20$, $e > 0.35$). Variable: argument of the periastron.

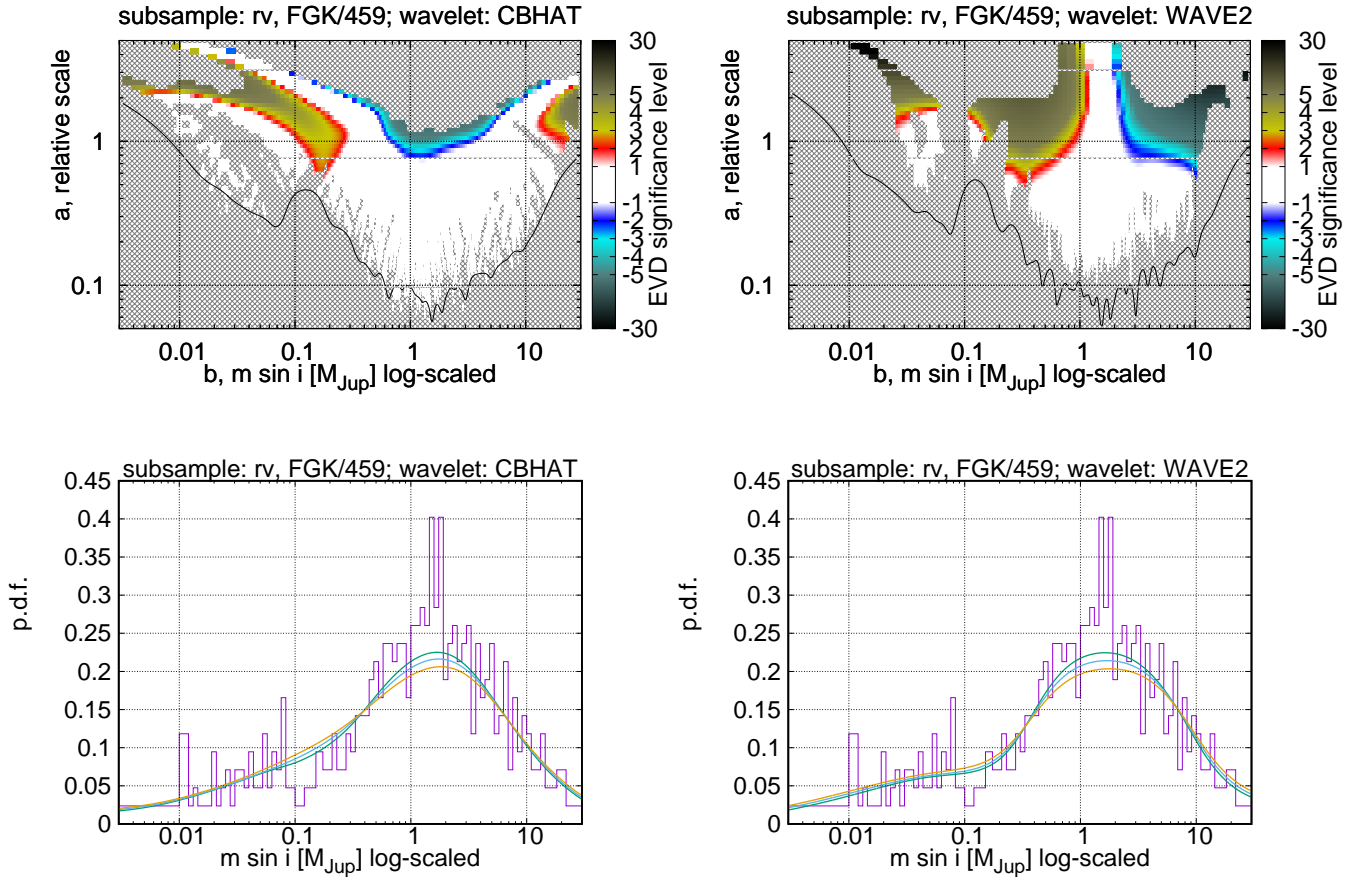


Figure 9. Subsample: RV detection method, FGK-type host stars, $N = 459$. Variable: planet minimum mass $m \sin i$.

independent follow-up Doppler *confirmation*, which is much easier than to make a *detection*.

We did not detect any small-scale details in the exoplanetary mass distribution.

6 SOME SELF-CRITICISM CONCERNING THE SIGNIFICANCE ESTIMATES

Unfortunately, the issue of a hidden p-hacking effect often appears very difficult to overcome completely. The numeric significance levels reported above are still not entirely free from an overestimation caused by multiple testing.

First of all, we always considered *two* wavelet transforms simultaneously, WAVE2 and CBHAT. Hence, our analysis hiddenly involved *two* comparison tests, on the *same* distribution. The number of false alarms should then appear larger than expected from just a single wavelet transform. In fact, our test involved the maximum between *two* distinct test statistics, namely $\max(z_{\text{WAVE2}}, z_{\text{CBHAT}})$, rather than the maximum of just a single $z(a, b)$.

Assuming that the maxima on the WAVE2 and CBHAT wavelet maps are uncorrelated with each other, we should roughly double the FAP estimate. Then, using this assumption and the definition (5), we can derive a correction to the

g -level:

$$\begin{aligned} \text{FAP} &= 2[1 - \Phi(g)], & \text{FAP}' &= 2\text{FAP}, \\ g' &= \Phi^{-1}\left(1 - \frac{\text{FAP}'}{2}\right) = \Phi^{-1}[2\Phi(g) - 1], \end{aligned} \quad (9)$$

For the subfamily $P = 300 - 600$ d we obtained in Sect. 5.1 the following detection significances in our CBHAT analysis: $g = 2.0$ (left concavity), $g = 3.4$ (central convexity), and $g = 2.1$ (right concavity). Formula (9) transforms these levels to the following: $g' = 1.6$, $g' = 3.2$, and $g' = 1.8$. The central convexity still remains pretty convincing, but the side separations appear to have just a marginal significance.

For the CKS radii distribution we obtain with CBHAT: $g > 5$ (left maximum), $g = 1.5$ (central gap), $g > 5$ (right maximum), and with WAVE2: $g = 1.6$ (descent to the gap) and $g = 2.0$ (uprise out of the gap). Using (9), this is corrected to: $g' > 5$ (left maximum), $g' = 1.1$ (central gap), $g' > 5$ (right maximum), $g' = 1.2$ (descent to the gap) and $g' = 1.6$ (uprise out of the gap). We can see that the gap becomes insignificant.

But from the other side, the WAVE2 and CBHAT wavelet maps should be correlated: if a pattern is detected by one of the wavelets, the other wavelet should likely reveal something unusual too. Therefore, the correction (9) is prob-

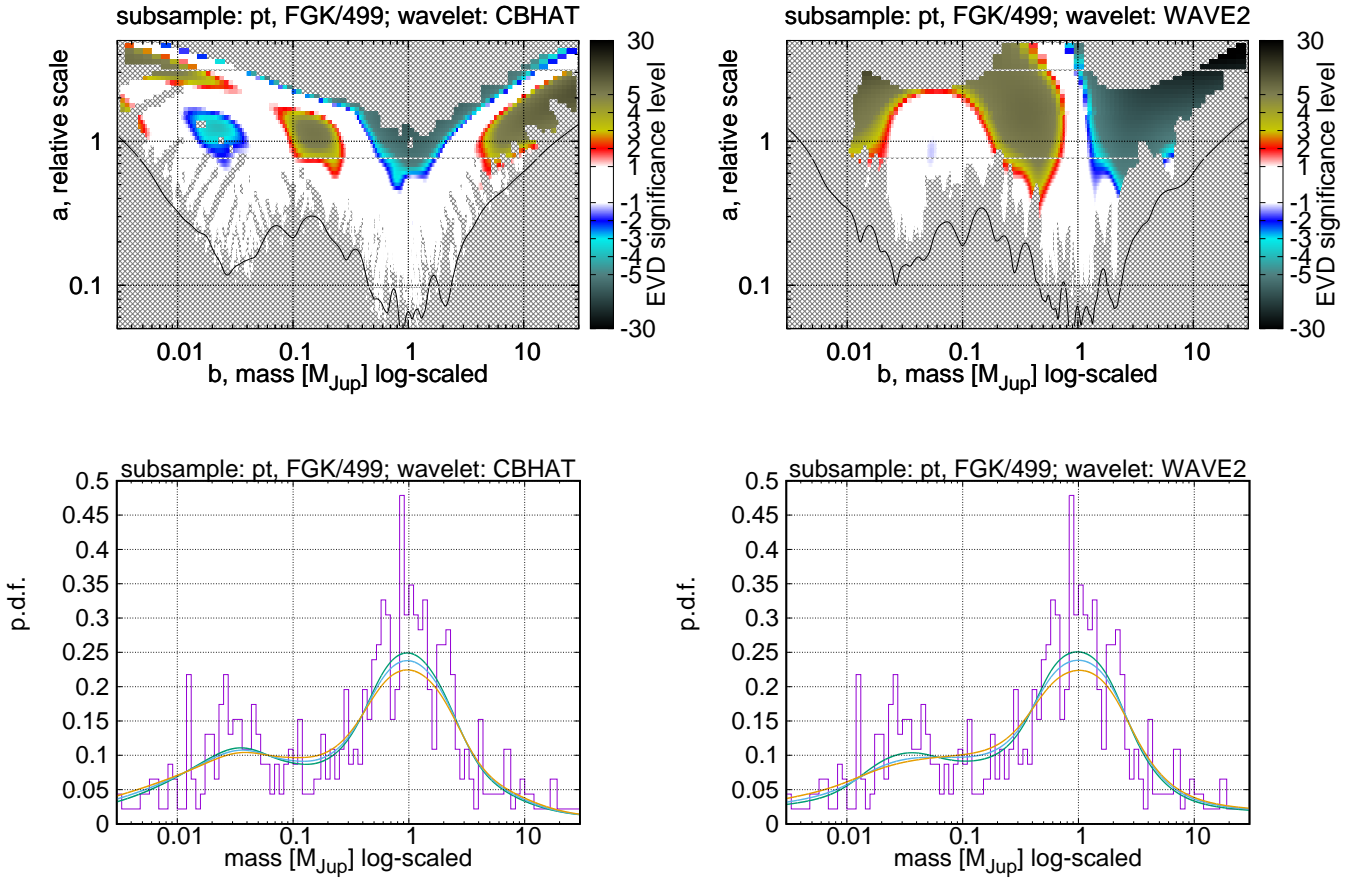


Figure 10. Subsample: Primary transit detection method, FGK-type host stars, $N = 499$. Variable: planet mass m .

ably too conservative. Moreover, our FAP estimate (4) was made conservative by design, because should tend to overestimate the actual FAP. It might seem likely that these effects could in turn compensate each other, so the uncorrected g -levels might be more realistic than g' from (9).

But more difficulties appear because we actually need the significance of *combined* patterns that involve *several* elementary structures on the wavelet maps. For example, to ensure that the subfamily $P = 300 - 600$ d does exist, we needed the whole triplet “concavity-concavity-concavity” to be confirmed as a whole. Just a single central concavity without side concavities is notable, but we would not classify it as a “subfamily”, because a subfamily should be separated in some way from the background planets. Without a separation, it should be interpreted just as relatively abrupt PV/WJ transition, but not as a separate family.

Similarly, when detecting the bimodality in the radii distribution, we needed to ensure the significance of the triplet “convexity-concavity-convexity” as a whole (in CBHAT) or of the doublet “descent-uprise” as a whole (in WAVE2). Without that, we cannot claim the two-family distribution structure.

The FAP of a doublet, or of a triplet, or of a general n -tuple set, cannot be expressed via FAPs for their individual elements. More detailed discussion of this issue is given

in (Baluev 2013b) respectively to the period search in time series. Unfortunately, a more rigorous solution to this issue involved too complicated theory and heavy computations. This is currently not feasible in our present task, so we did not incorporate anything beyond the single-component significance.

7 CONCLUSIONS AND DISCUSSION

On the basis of the analysis presented above, we draw two main conclusions concerning the exoplanetary distributions:

(i) There is a remarkable statistical support in favour of a narrow subfamily of giant exoplanets within the range $P = 300 - 600$ d. This subfamily seems to be separated from the rest of the sample by p.d.f. concavities on both sides (but this does not necessarily imply bimodality). Most probably, this subfamily has a connection with the iceline barrier effect in a protoplanetary disk. But to our knowledge, current theory work on planet formation did not predict such a family yet. Curiously, this subfamily appears to overlap well with the habitable zone for a solar-type star.

(ii) There is some statistical support in favour of the “evaporation valley” in the planet radii distribution of the CKS sample. But significance of this feature reported in

other works seems to be overestimated. That high significance appeared irreproducible in our work.

We highlight additionally, that although any “absolute” statistical significance is always difficult to estimate adequately, the “relative” comparison is easier. For example, it follows from our analysis that the “evaporation valley” is notably less confident than the 300 – 600 d subfamily.

The distributions of exoplanetary masses and orbital eccentricities did not reveal new features. The angular distribution of orbital pericenters is consistent with the uniform one, suggesting that there is no detectable selection effects with respect to this parameter.

ACKNOWLEDGEMENTS

This work was supported by the Russian Foundation for Basic Research, project 17-02-00542 A, and by the programme P7 of the Presidium of Russian Academy of Sciences.

REFERENCES

- Anglada-Escudé G., et al., 2016, *ApJ*, 830, 74
 Baluev R. V., 2008, *MNRAS*, 385, 1279
 Baluev R. V., 2013a, *MNRAS*, 429, 2052
 Baluev R. V., 2013b, *MNRAS*, 436, 807
 Baluev R. V., 2015, *MNRAS*, 446, 1493
 Baluev R. V., 2017, *Astron. & Comp.*, submitted, arXiv.org:1711.07820
 Cumming A., 2010, in Seager S., ed., *Exoplanets*. University of Arizona Press, Tucson, Chapt. 9, pp 191–214
 Forveille T., et al., 2011, arXiv:1109.2505
 Foster G., 1995, *AJ*, 109, 1889
 Foster G., 1996, *AJ*, 111, 541
 Fulton B. J., et al., 2017, *AJ*, 154, 109
 Gelman A., Loken E., 2014, *American Scientist*, 102, 460
 Gregory P. C., 2011, *MNRAS*, 415, 2523
 Hara N. C., Boué G., Laskar J., Correia A. C. M., 2017, *MNRAS*, 464, 1220
 Hartigan J. A., Hartigan P. M., 1985, *Annals of Statistics*, 13, 70
 Hasegawa Y., Pudritz R. E., 2013, *ApJ*, 778, 78
 Hayashi C., 1981, *Prog. Theor. Phys. Suppl.*, 70, 35
 Ida S., Lin D. N. C., 2004, *ApJ*, 604, 388
 Ida S., Lin D. N. C., 2008, *ApJ*, 685, 584
 Johnson J. A., et al., 2017, *AJ*, 154, 108
 Mayor M., Queloz D., 1995, *Nature*, 378, 355
 NASA 2017, *NASA Exoplanets Archive*, exoplanetarchive.ipac.caltech.edu/
 Owen J. E., Wu Y., 2017, *ApJ*, 847, 29
 Petigura E. A., et al., 2017, *AJ*, 154, 107
 Roberts D. H., Lehar J., Dreher J. W., 1987, *AJ*, 93, 968
 Robertson P., Mahadevan S., Endl M., Roy A., 2014, *Science*, 25, 440
 Robertson P., Mahadevan S., Endl M., Roy A., 2015, *Science*, 347, 1080
 Roques F., Schneider J., 1995, *The Extrasolar Planets Encyclopaedia*, www.exoplanet.eu
 Schlaufman K. C., Lin D. N. C., Ida S., 2009, *ApJ*, 691, 1322
 Schwarzenberg-Czerny A., 1998, *Baltic Astron.*, 7, 43
 Skuljan J., Hearnshaw J. B., Cottrell P. L., 1999, *MNRAS*, 308, 731
 Süveges M., 2014, *MNRAS*, 440, 2099
 Tadeu dos Santos M., Silva G. G., Ferraz-Mello S., Michtchenko T. A., 2012, *Celest. Mech. Dyn. Astron.*, 113, 49

Vogt S. S., Butler R. P., Rivera E. J., Haghighipour N., Henry G. W., Williamson M. H., 2010, *ApJ*, 723, 954

Vogt S. S., Butler R. P., Haghighipour N., 2012, *Astron. Nachr.*, 333, 561

Wright J. T., Upadhyay S., Marcy G. W., Fischer D. A., Ford E. B., Johnson J. A., 2009, *ApJ*, 693, 1084

This paper has been typeset from a $\text{\TeX}/\text{\LaTeX}$ file prepared by the author.